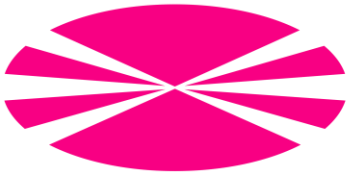

UNIVERSIDADE
DA CORUÑA

INTRODUCTION TO MARINE COMPUTATIONAL FLUID DYNAMICS

PROF. ANNE MARIE ELISABETH GOSSET

PROF. MARCOS LEMA RODRÍGUEZ

SEMESTER PROJECT

BY

AKINMULEWO DANIEL

NWAFOR OGECHUKWU

SUSTAINABLE SHIP AND SHIPPING 4.0

HIGHER POLYTECHNIC UNIVERSITY COLLEGE

UNIVERSITY OF A CORUÑA

Table of Contents

1.0. INTRODUCTION 3

2.0. APPROXIMATIONS AND MODELS 4

2.1. TURBULENCE MODELLING 4

2.1.1. k-ω SHEAR STRESS TRANSPORT (k-ω SST) 4

3.0. PRE-PROCESSING 5

3.1. MESH RESOLUTION AND DOMAIN SIZE 5

3.2. TIME STEP 7

3.3. INITIAL AND BOUNDARY CONDITIONS 7

4.0. PROCESSING 9

4.1. PARAMETRIZATION OF THE SOLVER AND DISCRETIZATIONS SCHEMES 9

4.2. SOLUTION MONITORING 10

5.0. POST-PROCESSING AND RESULTS 13

5.1. FLOW VISUALIZATION 13

5.2. COEFFICIENTS 14

6.0. VERIFICATION, VALIDATION AND CONCLUSIONS 17

7.0. REFERENCES 22

List of Figures

Figure 1.0 Design parameters for NACA XXXX hydrofoil. 3
Figure 2.0 Law of the Wall 4
Figure 3.0 NACA0015 Geometry Domain 5
Figure 4.0 Case Study(a): NACA0015 Figure 4.0 Case Study(b): NACA0015 5
Figure 5.0 BlockMesh C-type(a) Figure 6.0 BlockMesh C-type(b) 6
Figure 7.0 Mesh Evolutions 6
Figure 8.0 Residuals for Standard and Scalable Wall Functions 10
Figure 9.0 Drag and Lift coefficients using Standard Wall Function 10
Figure 10.0 Drag and Lift coefficients using Scalable Wall Function 11
Figure 11.0 Drag and Lift coefficients Resolved Boundary Layer 11
Figure 12.0 Residuals for Standard Wall (SIMPLE FOAM) 11
Figure 13.0 Drag and Lift Coefficients Standard Wall (SIMPLE FOAM) 12
Figure 14.0 Simulation of 2D hydrofoil Figure 15.0 Simulation of 2D hydrofoil (Resolved BL) . 13
Figure 16.0 Simulation of 2D hydrofoil (Standard Wall) 13
Figure 17.0 Simulation of 2D hydrofoil (Scalable Wall) 13
Figure 18.0 Standard Wall Coefficients 14
Figure 19.0 Scalable wall Coefficients 15
Figure 20.0 Hydrodynamic Coefficients Comparison with Angles of Attack 18
Figure 21.0 Lift and Drag Experimental Results 18

1.0. INTRODUCTION

It is critical and important to be able to precisely estimate vortex shedding around a hydrofoil, especially at high Reynolds numbers and to estimate the hydrodynamic properties such as lift and drag, which play an important role in ship maneuverability. Turbulence models used in numerical simulations have a significant impact on flow separation and hydrodynamic loading, influencing the overall accuracy of numerical simulations. In this analysis the k-ω Shear Stress Transport model is investigated in two dimensional configurations using standard Reynolds Average Navier-Strokes (RANS) equations. The focus is on the standard 4-digit NACA0015 hydrofoil-like rudder, and the simulations are conducted at a Reynolds number of 7.0×10^5.

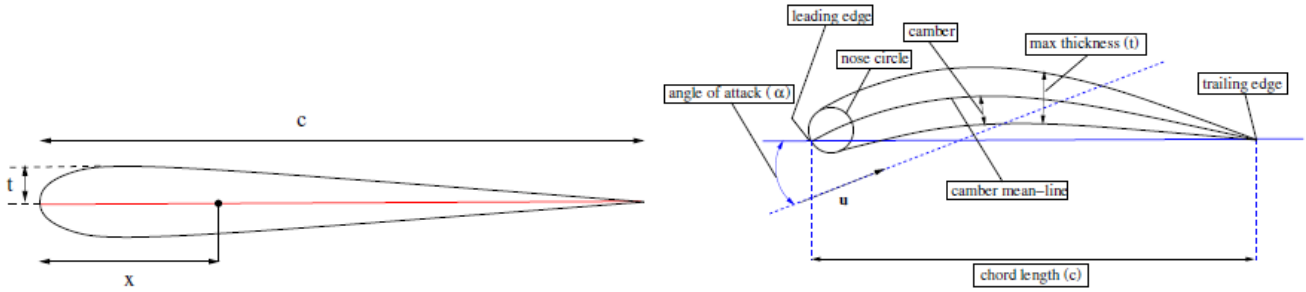

Figure 1.0 Design parameters for NACA XXXX hydrofoil.

The effects of the flow separation and vortex shedding pattern is investigated at an angle of attack AoA (7°) along with the prediction ability of the turbulence model. The Standard wall function, Scalable wall function and No wall function are used for the treatment of the Boundary Layer, and the results is compared to the experimental result.

In order to determine the changes in the hydrodynamic coefficient with respect to the domain size, two domain sizes are defined to evaluate these dependencies. Six mesh evolutions are also defined to determine the lift coefficients C_L, drag coefficients C_D, pressure coefficients C_P, and the flow visualization results obtained.

This report therefore analyses the impacts of meshes on the prediction accuracy of RANS simulations with the above listed wall treatment functions, and the relative size of the domain in steady and unsteady state using **Openfoam** CFD program.

2.0. APPROXIMATIONS AND MODELS

2.1. TURBULENCE MODELLING

The Reynolds Averaged Navier–Stokes (RANS) equations, obtained by time averaging the NS equations, are usually employed to simulate turbulent industrial flows. These equations need a closure to compute an unknown, the Reynolds tensor constituted by the double correlation of the turbulent fluctuations, that derives from the convective term of the NS equations. The task of a turbulence model is to close the RANS equations by computing the components of the Reynolds stress tensor. For this analysis, the RANS turbulence model is used.

2.1.1. k-ω SHEAR STRESS TRANSPORT (k-ω SST)

To model eddy viscosity, it solves k-ω in the inner part of the boundary layer and transition to k-ε in the free stream region. The SST formulation regulates the transition between the models. Menter(8) introduced a blending function which controls the switching between ω and ε equations.

- The Standard Wall Function: y^+ has been maintained in the buffer region for the simulation between $30 \leq y^+ \leq 300$ such that the wall functions set the correct ω and k at the wall for each first cell.
- The Scalable Wall Function: y^+ has been maintained in the buffer region for the simulation between $1 \leq y^+ \leq 300$
- Resolved Boundary Layer: y^+ has been maintained down to the viscous sublayer (no wall function) $y^+ \leq 6$.

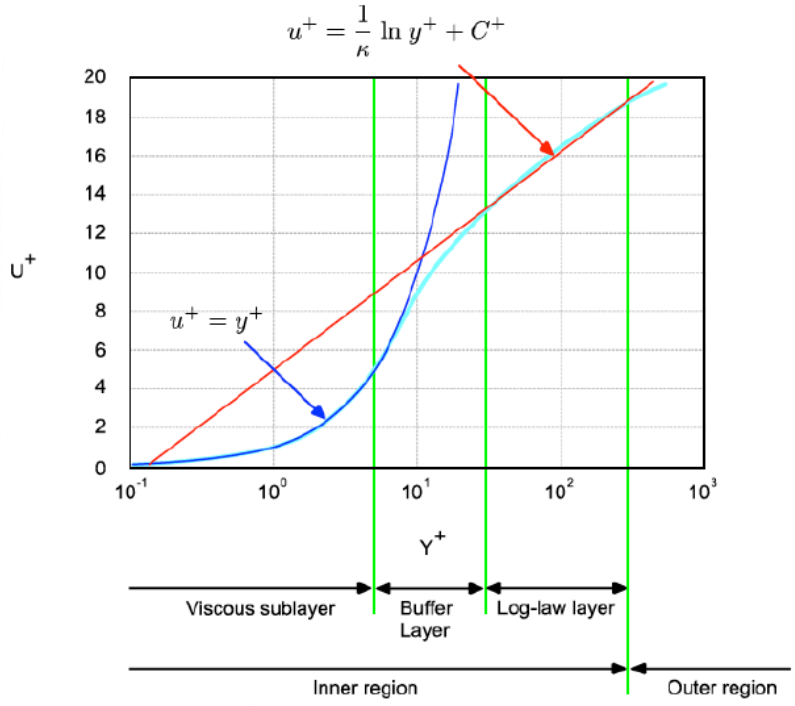

Figure 2.0 Law of the Wall

3.0. PRE-PROCESSING

3.1. MESH RESOLUTION AND DOMAIN SIZE

A Multiblock structured mesh offers better computational efficiency than the unstructured meshes which, on the other hand, are more flexible for complex geometries. The NACA0015 hydrofoil is a less complex geometry and the multiblock structured mesh has been adapted to allow for more control over the generation of computational mesh. It has provided more flexibility near the sharp corners, and to conformed well to the underlying geometry.

A block-C-type mesh is applied to the computational domain. Sharp gradients resulting from fast changes in the flow physics on the surface and in the wake region of the hydrofoil cause quality orthogonal cells to cluster. With excellent hexahedral elements, it also provided a smooth transition from the hydrofoil surface to the outer flow field.

For the different wall functions used in the analysis, two domain sizes are defined with six different mesh evolutions in order to evaluate the sensitivity to the hydrodynamic coefficients.

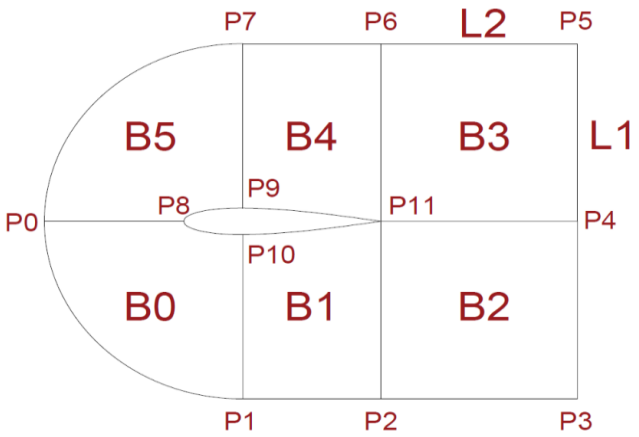

Figure 3.0 NACA0015 Geometry Domain

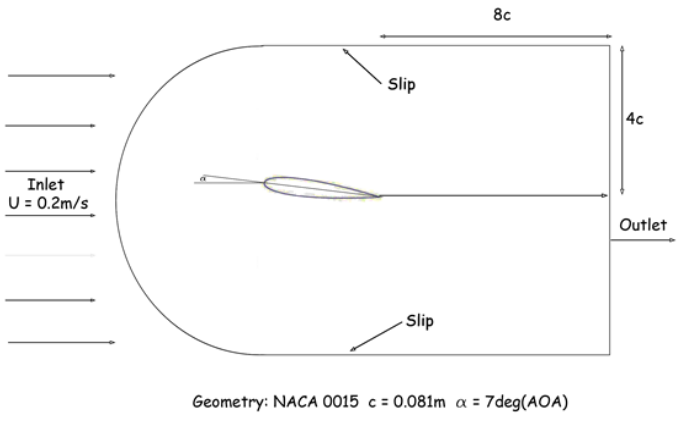

Figure 4.0 Case Study(a): NACA0015

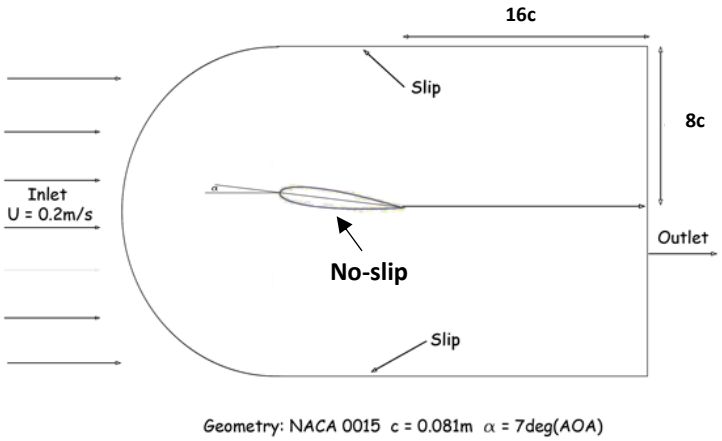

Figure 4.0 Case Study(b): NACA0015

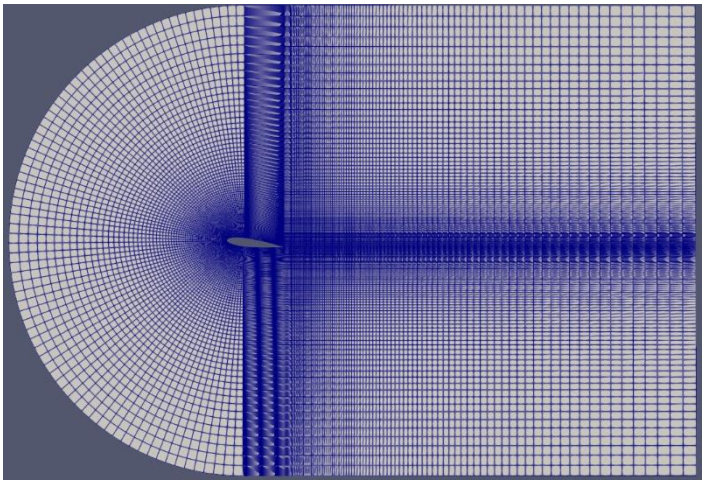

Figure 5.0 BlockMesh C-type(a)

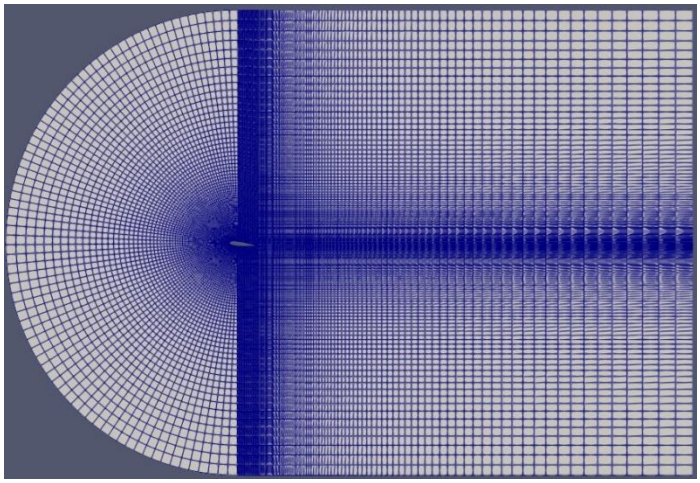

Figure 6.0 BlockMesh C-type(b)

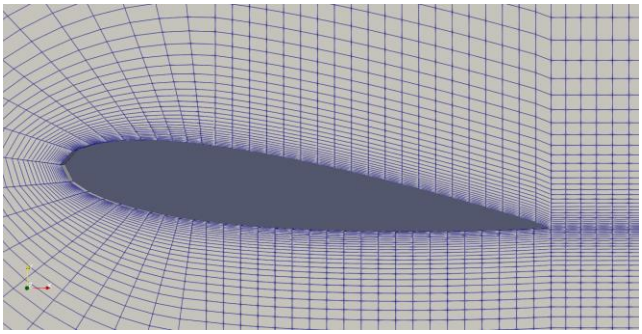

Hexahedral: 10000

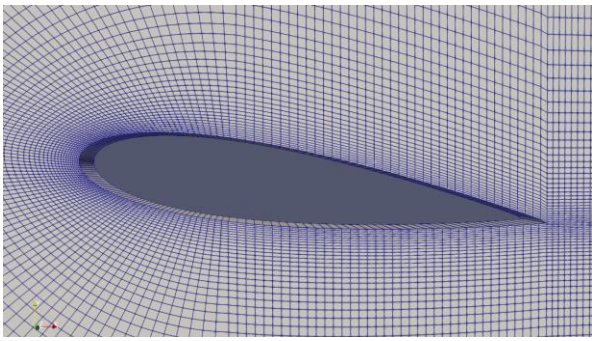

Hexahedral: 25120

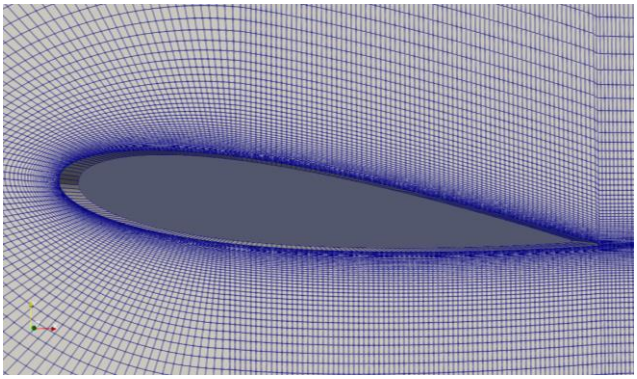

Hexahedral: 37038

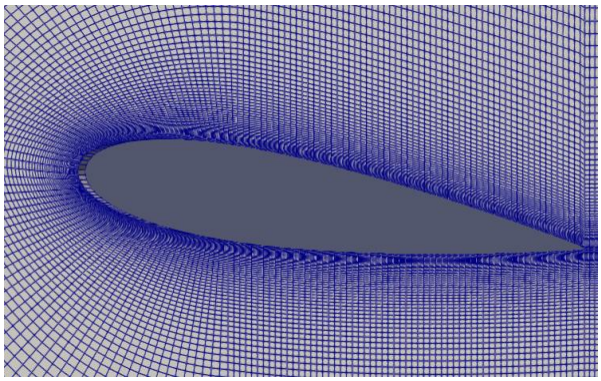

Hexahedral: 40000

Figure 7.0 Mesh Evolutions

Standard and Scalable Wall-Function Block Mesh properties

No of Cells	Mesh Type	delta_T	Non-orthogonality		Max Skewness		Max CFL
			8c	16c	8c	16c	
10000	Hexahedral	0.01	6.85	6.85	1.76	1.76	0.7
15000	Hexahedral	0.01	7.58	7.4	1.25	1.25	0.72
20020	Hexahedral	0.01	7.82	7.47	1	1	0.79
25120	Hexahedral	0.01	8.66	8.8	0.62	0.62	0.82
30060	Hexahedral	0.01	8.69	8.67	0.64	0.55	0.94
40000	Hexahedral	0.008	9.02	9	0.81	0.78	0.99

Table 1.0: Mesh Properties

Resolved Boundary Layer Wall-Function Block Mesh properties using domain size of 4c around the hydrofoil and 8c downstream.

No of Cells	delta_T	Cl	Cd	Cl/Cd	y+min	y+max	y+avg
37042	0.00001	0.69	0.024	28.75	0.04	1.5	0.59

Table 2.0: Mesh Properties

3.2. TIME STEP

The values of the time step size(Δt) are chosen so that the solution's overall numerical stability is preserved. The Courant number is monitored and adjusted to be less than one in order to maintain stability. Maintaining the overall correctness of the solution still necessitates an initial accurate time step estimation. As a result, the initial time step has been accurately estimated after observing the initial time set up.

3.3. INITIAL AND BOUNDARY CONDITIONS

The flow field is assumed to be fully turbulent, and the transition from laminar to turbulent regime inside the boundary layer is not explicitly modeled on the upper and lower surface of the hydrofoil.

From the non-dimensional Reynoids number (7.0 x10^5), two approaches were implemented for the calculations:

- **Assuming the fluid to be water at room temperature:**
- Kinematic viscosity ν: 1 x 10^{-6} kg/m.s
- Constant inflow velocity u_∞ = 8.641m/s
- **Assuming low constant inflow velocity:**
- Dynamic viscosity ν = 2.32x10^{-8} kg/m.s,
- constant inflow velocity of u_∞= 0.2 m/s

Using the two approaches, the value of the hydrodynamic coefficients has little to no differences since the major factor that determine the property of the flow is the Reynoids number. However, running the simulation with a higher velocity increases computational time and is highly expensive. The Law of the wall are utilized to relax the concentration of mesh resolution near the hydrofoil surface and the fixed value has been used for the Resolved BL case.

Boundary Conditions		Initial Conditions				
Patch	B.C	0/U	0/p	0/k	0/ω	0/nut
Inlet	Inlet	Fixed Value: uniform (0.2, 0, 0)	ZeroGradient	Fixed Value: uniform 0	Fixed Value: uniform 258.62	Calculated: uniform 2.3e-8
Outlet	Outlet	ZeroGradient	Fixed Value: uniform 0	inletOutlet InletValue: 6e-6	inletOutlet InletValue: 258.62	Calculated: uniform 2.3e-8
Top	Slip	Symmetry	Symmetry	Symmetry	Symmetry	Symmetry
Bottom	Slip	Symmetry	Symmetry	Symmetry	Symmetry	Symmetry
Hydrofoil	Wall	Fixed Value: uniform(0, 0, 0)	ZeroGradient	KqRWallFunction: uniform 6e-6	omegaWallFunction: uniform 258.62	nutkWallFunction: uniform 2.3e-8
Front	Empty	Empty	Empty	Empty	Empty	Empty
Back	Empty	Empty	Empty	Empty	Empty	Empty
Turbulence intensity				1%		

Table 3.0: Boundary and Initial Conditions

4.0. PROCESSING

4.1. PARAMETRIZATION OF THE SOLVER AND DISCRETIZATIONS SCHEMES

A PIMPLE (combination of PISO-SIMPLE) algorithm is employed. The equations are discretized in a finite volume technique and integrated over Control Volumes(CV) using the Green-Gauss divergence theorem. Thus, volume integrals are transformed into surface integrals of the CV.

- Time discretization :
  First order, bounded, implicit discretization (Euler) is employed for the time discretization. The challenge with this scheme, is it high diffusive properties which overestimate the lift and drag coefficient.
- Gradient Schemes:
  The grad Schemes interpolate the values for the gradient terms in the differential equations. Second order, least squares is employed, for better stability and robustness, the 'cellLimited' versions is used and a 'Limiter coefficient' of 1.0 for full boundedness/limiting of values.
- Divergence Schemes:
  Gauss linearUpwind v ∇u**:** second-order, upwind, bounded, is a good choice for stable second-order linear scheme, and it was employed.
- Laplacian Scheme:
  For the solution of diffusion term in the NS equation, second order, Gauss linear limited with limiter value 1 is employed.

Non-orthogonal correction is realized for all equations as solver stability is not trivial owing to the utilization of computational mesh. To solve the systems of governing equations, Geometric Agglomerated Algebraic Multigrid (GAMG) solver is employed. The solution time is reduced by applying DIC as a smoother, which damp the oscillations in the solution and enhances convergence.

Also due to the no evidence of vortex shedding or Von Karman Street, the simulation is also conducted in Steady state using the SimpleFoam solver. The solver implements the SIMPLE Algorithm.

Using the SimpleFoam Solver, the under-relaxation factor is introduced to suppress oscillations and divergence, values for pressure field, velocity and turbulence equations are set to be:

p = 0.3,

U = 0.7;

k = 0.7;

omega = 0.7;

4.2. SOLUTION MONITORING

To monitor solution convergence, the tolerance for the pressure field is set to 10e-6 and 10e-8 for velocity. For the turbulence model, the tolerance is set to 10e-8.

Solutions can be considered converged when the flow field and scalar fields are no longer changing or maintaining a mean periodic oscillatory motion in unsteady solutions.

The residual for the pressure field converges at a tolerance of 10e-4, this shows flow convergence against set value of 10e-6. This is similar to the velocity field; the solution converges at a tolerance of 10e-6.

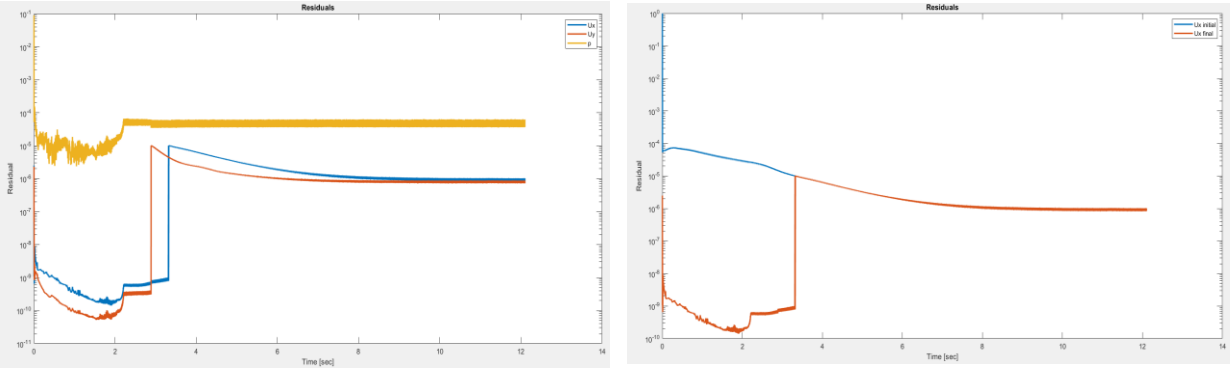

Figure 8.0 Residuals for Standard and Scalable Wall Functions

Also using either wall function or resolved BL of the turbulence model, no oscillations in the hydrodynamic coefficients are observed, which is a manifestation of attached flow around the hydrofoil and shows a good converge solution.

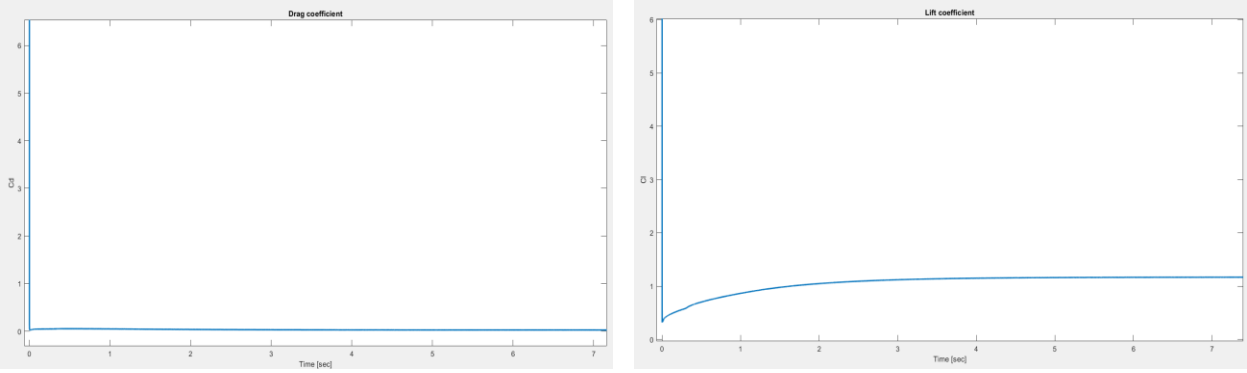

Figure 9.0 Drag and Lift coefficients using Standard Wall Function

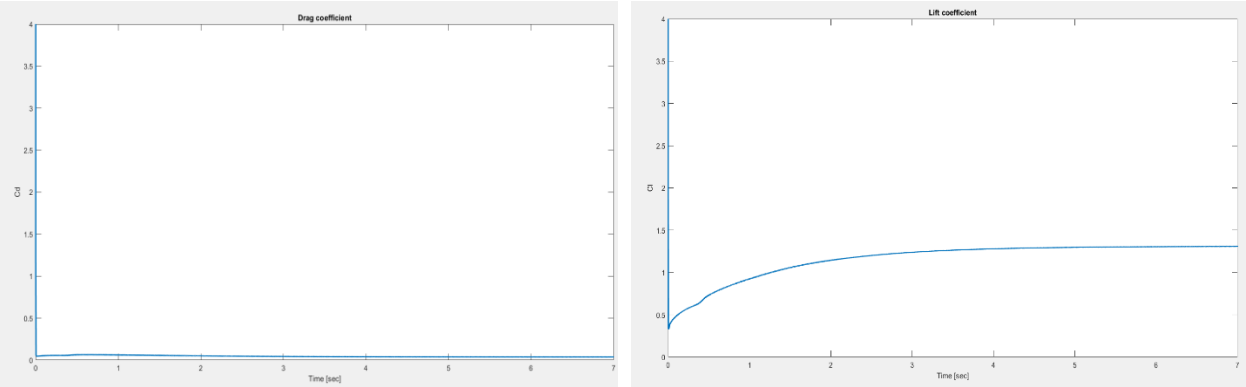

Figure 10.0 Drag and Lift coefficients using Scalable Wall Function

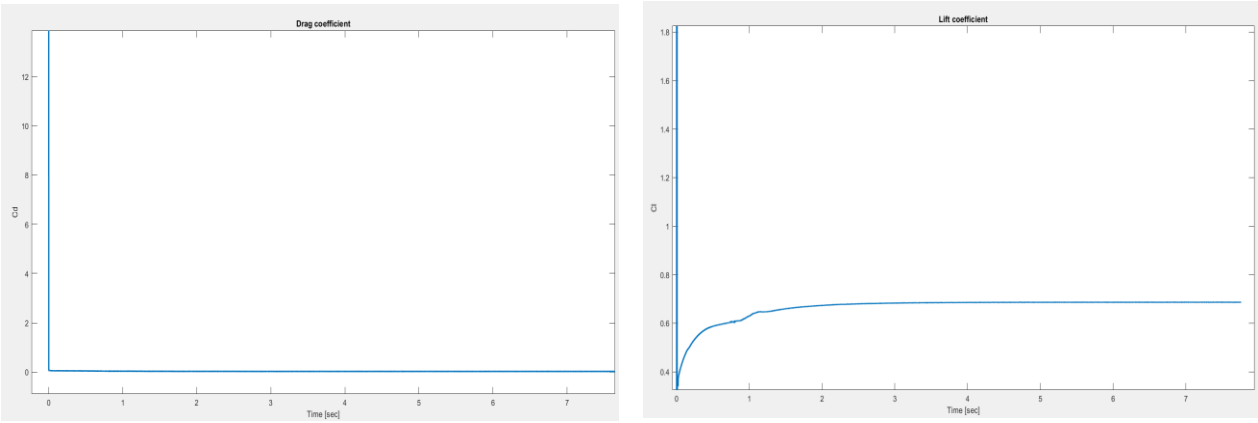

Figure 11.0 Drag and Lift coefficients Resolved Boundary Layer

Using SIMPLE Foam Solver for the final refined mesh, the residuals plot in figure 12.0 shows an oscillating motion with little deviation in the hydrodynamic coefficient when compared to the unsteady state.

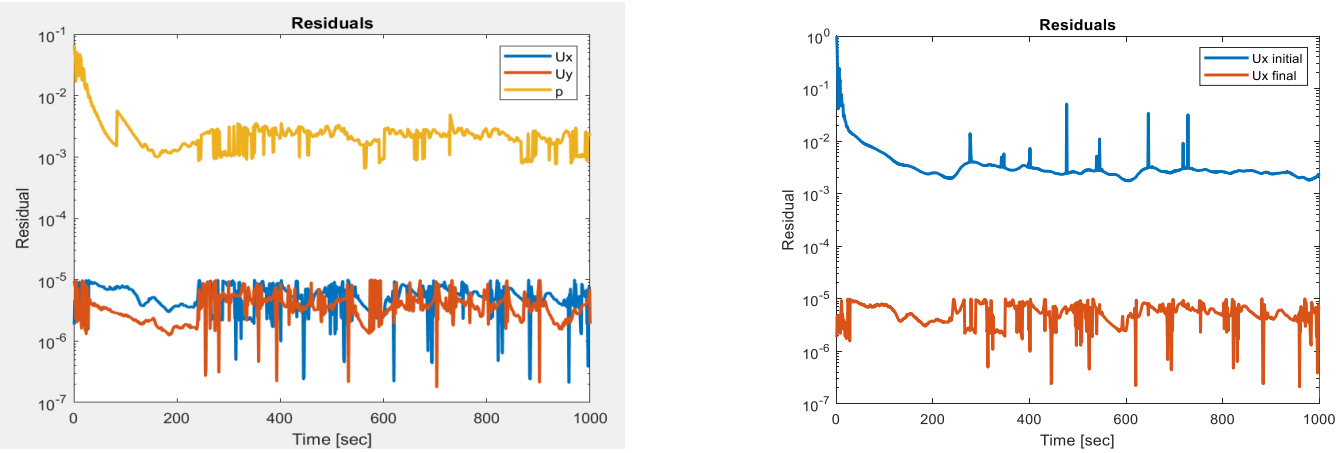

Figure 12.0 Residuals for Standard Wall (SIMPLE FOAM)

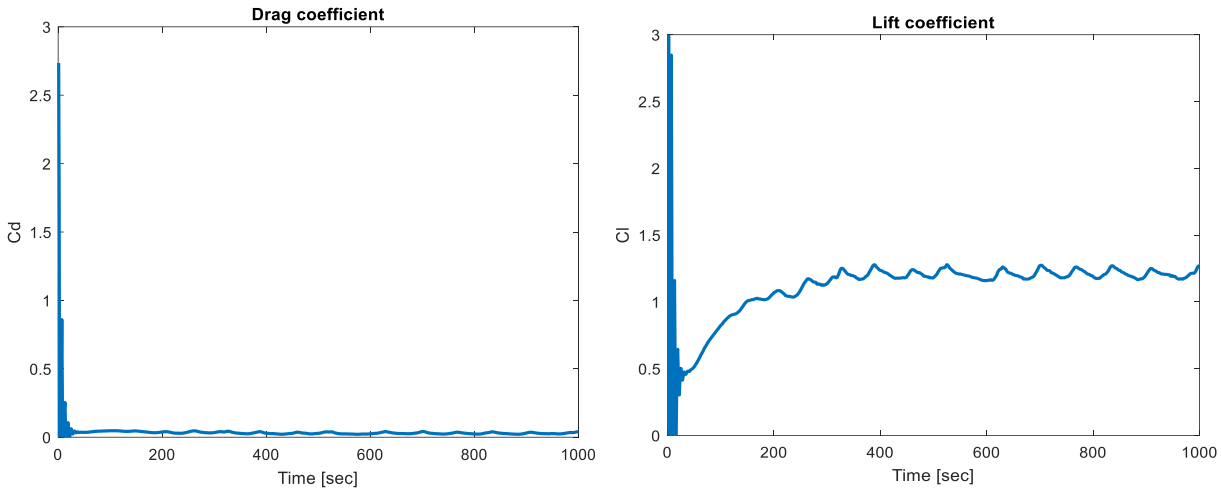

Figure 13.0 Drag and Lift Coefficients Standard Wall (SIMPLE FOAM)

5.0. POST-PROCESSING AND RESULTS

5.1. FLOW VISUALIZATION

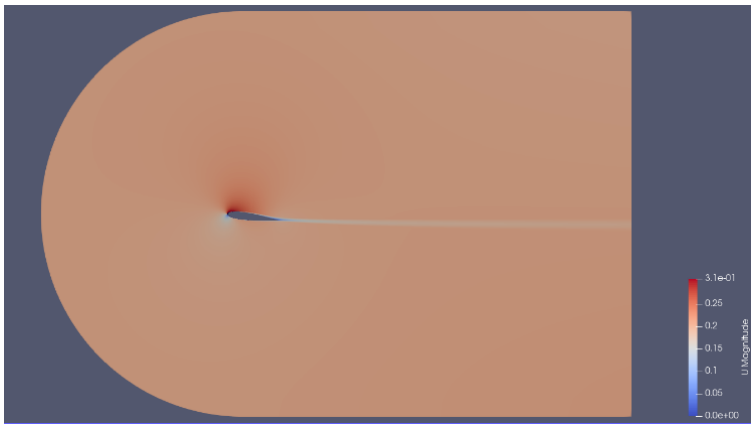

Figure 14.0 Simulation of 2D hydrofoil

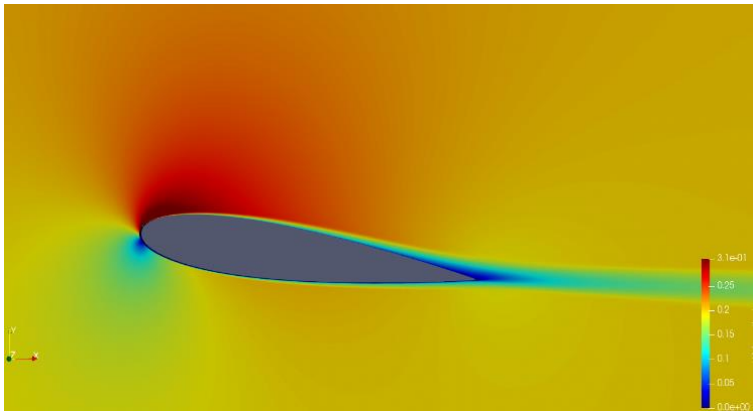

Figure 15.0 Simulation of 2D hydrofoil (Resolved BL)

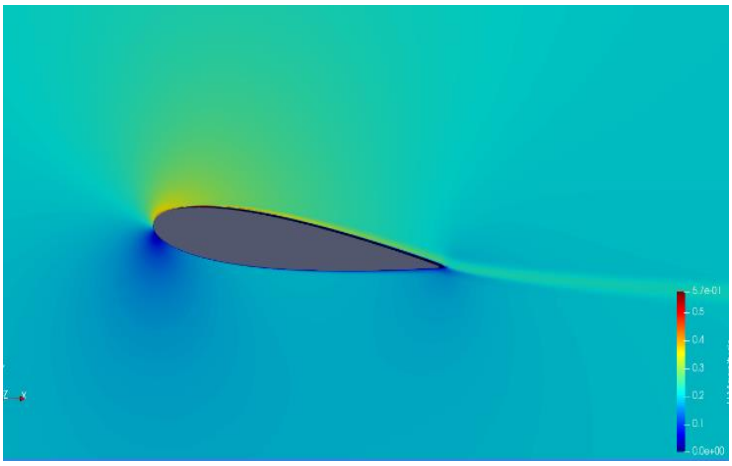

Figure 16.0 Simulation of 2D hydrofoil (Standard Wall)

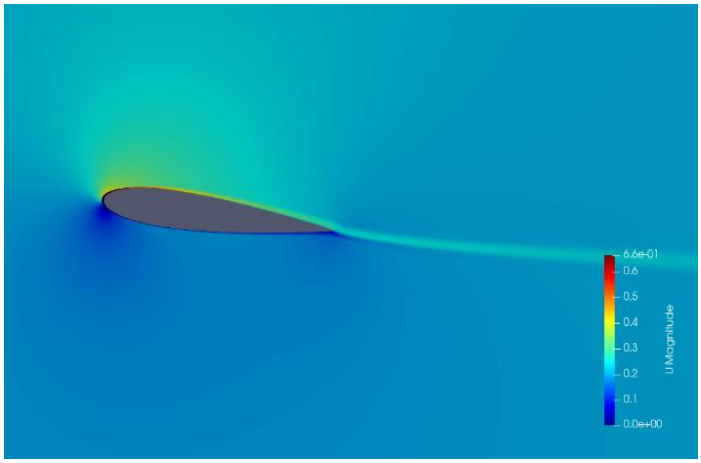

Figure 17.0 Simulation of 2D hydrofoil (Scalable Wall)

5.2. COEFFICIENTS

In order to analyze the effect of the domain size on the hydrodynamic coefficients, six mesh evolutions are defined and are simulated using both the standard and scalable wall treatment function and comparing the results to the resolved boundary layer. Also, the difference in the hydrodynamic coefficients obtained is compared to the final refined mesh for each case and expressed in terms of percentage.

For the smaller domain size with length of downstream of 8c (i.e. 8 times the chord length), the hydrodynamic coefficient are as follows.

- The Standard Wall Function

No of Cells	delta_T	Cl	ΔCl [%]	Cd	ΔCd [%]	Cl/Cd	y+min	y+max	y+avg
10000	0.01	1.48	21	0.046	59	32.17	5.56	388.69	67.86
15000	0.01	1.35	11	0.041	41	32.93	12.3	181.58	56.44
20020	0.01	1.3	7	0.037	28	35.14	12.92	207.13	47.25
25120	0.01	1.21	-1	0.029	0.00	41.72	7.46	89.83	41.6
30060	0.01	1.22	0.00	0.029	0.00	42.07	2.82	94.89	43.76
40000	0.008	1.22	0.00	0.029	0.00	42.07	2.63	102.05	45.02

Table 4.0: Hydrodynamic Coefficients using Standard Wall Function

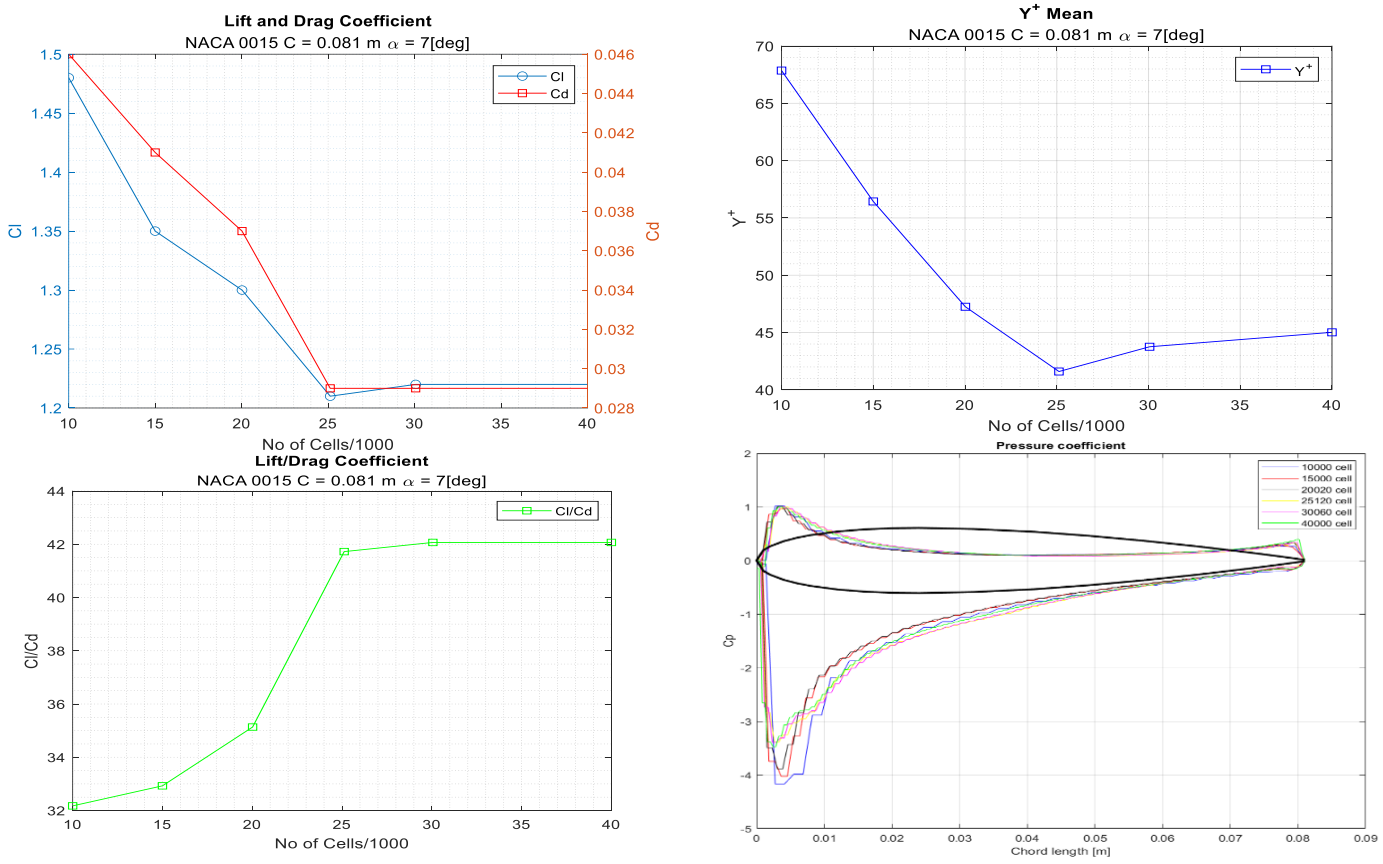

Figure 18.0 Standard Wall Coefficients

➢ The Scalable Wall Function

No of Cells	delta_T	Cl	ΔCl [%]	Cd	ΔCd [%]	Cl/Cd	y+min	y+max	y+avg
10000	0.01	1.47	24	0.052	73	28.27	5.09	160.46	74.33
15000	0.01	1.34	13	0.042	40	31.91	4.37	119.72	56.44
20020	0.01	1.28	8	0.036	20	35.56	3.81	92.93	43.02
25120	0.01	1.18	-1	0.031	3	38.07	4.95	86.29	42.55
30060	0.01	1.19	0.00	0.03	0.00	39.67	3.92	91.83	45.25
40000	0.008	1.19	0.00	0.03	0.00	39.67	1.54	69.92	29.94

Table 4.0: Hydrodynamic Coefficients using Scalable Wall Function

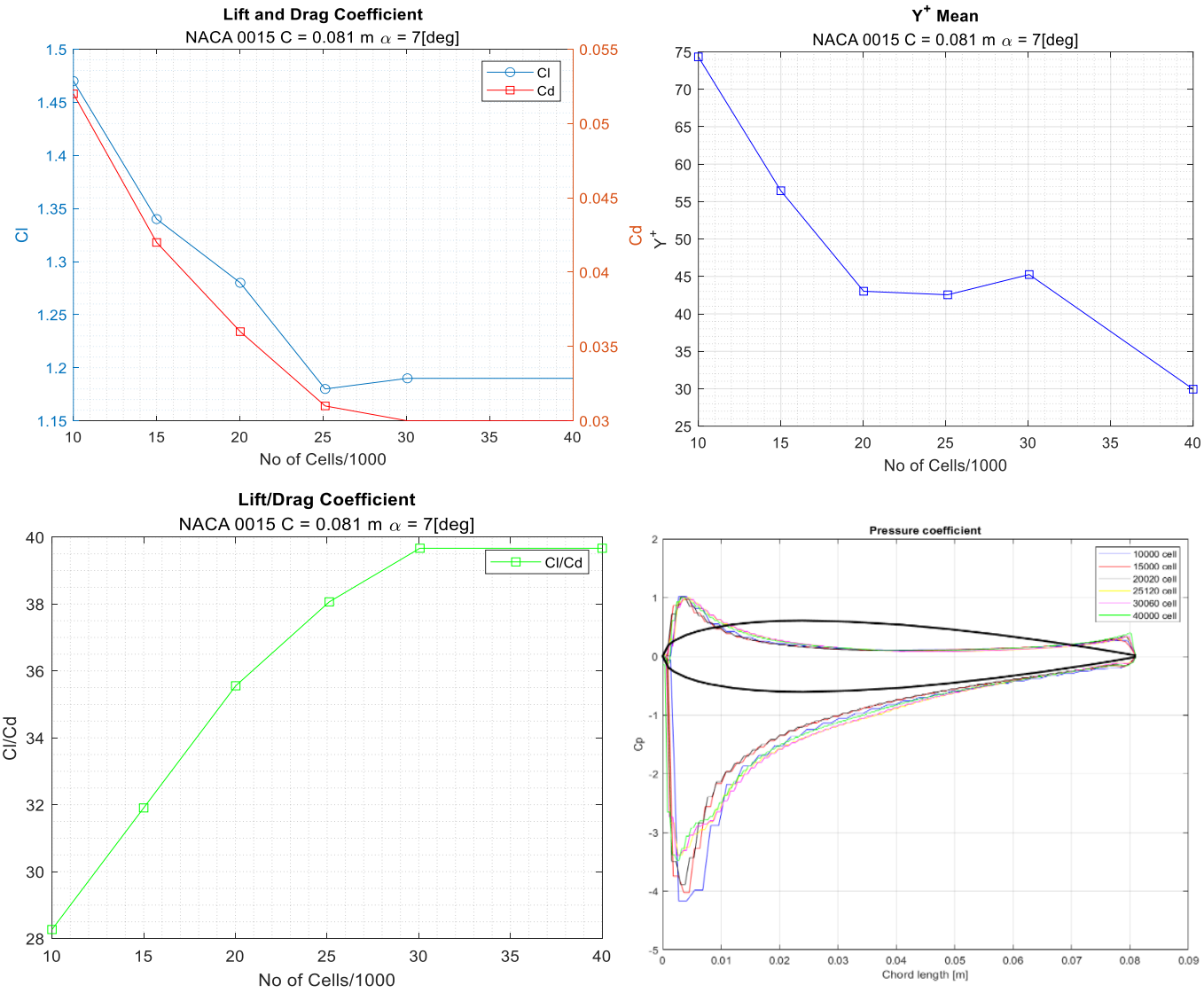

Figure 19.0 Scalable wall Coefficients

- From the different mesh evolutions, the solution becomes mesh independent at mesh size above 25000 cells.
- The values of the drag coefficient are sensitive to the wall treatment function. This is due to the fact the drag coefficient depends on the wall proximity. In order to determine a converge approximations for the drag coefficient, the average y+ for the 6 mesh evolutions were kept within the same range.
- Since there was no large variation in the hydrodynamic coefficient using the standard or scalable wall treatment function, another simulation was made for the large domain size using only the standard wall function

For the larger domain size with length of downstream of 16c (16 times the chord length), the hydrodynamic coefficient are as follows.

No of Cells	delta_T	Cl	ΔCl [%]	Cd	ΔCl [%]	Cl/Cd	y+min	y+max	y+avg
10000	0.01	1.42	13.6	0.086	274	16.51	12.57	338.36	64.65
15000	0.01	1.33	6.4	0.046	100	28.91	8.89	72.9	40.4
20020	0.01	1.33	6.4	0.34	47.83	3.91	10.15	72.3	40.9
25120	0.01	1.34	7.2	0.31	34.78	4.32	2.03	396.941	35.07
30060	0.01	1.23	-1.6	0.021	-8.69	58.57	1.4	216.72	45.19
40000	0.08	1.25	0.00	0.023	0.00	58.09	2.99	97.28	42.98

Table 5.0: Hydrodynamic Coefficients using Standard Wall Function

- The Resolved Boundary Layer

No of Cells	delta_T	Cl	Cd	Cl/Cd	y+min	y+max	y+avg
37042	0.00001	0.69	0.024	28.75	0.04	1.5	0.59

Table 6.0: Hydrodynamic Coefficients using Resolved Boundary Layer

- The Standard Wall Function in Steady State (SIMPLE FOAM)

No of Cells	delta_T	Cl	Cd	Cl/Cd	y+min	y+max	y+avg
40000	0.00001	1.27	0.039	32.56	1.19	104.72	34.31

Table 7.0: Hydrodynamic Coefficients using Standard Wall Layer in Steady-State

6.0. VERIFICATION, VALIDATION AND CONCLUSIONS

For final verification and validation, four approaches are used to justify the results of the hydrodynamic coefficient obtained.

- Comparison with different angles of attack.
- Comparison with domain size and geometry.
- Comparison with the experimental results.
- Comparison with wall treatment type.

- **Comparison with different angles of attack:**

  In close comparison with the different angles of attack of NACA 0015 profile (from other group), the relative hydrodynamics coefficients are plotted as a function of the mesh evolutions.

  It is clear from the figure below that the lift coefficient increases as the angle of attack increases. However, the drag coefficient also increases with the exemption to 8 deg AoA. This error is possibly due to the large variation in the wall proximity (average y+).

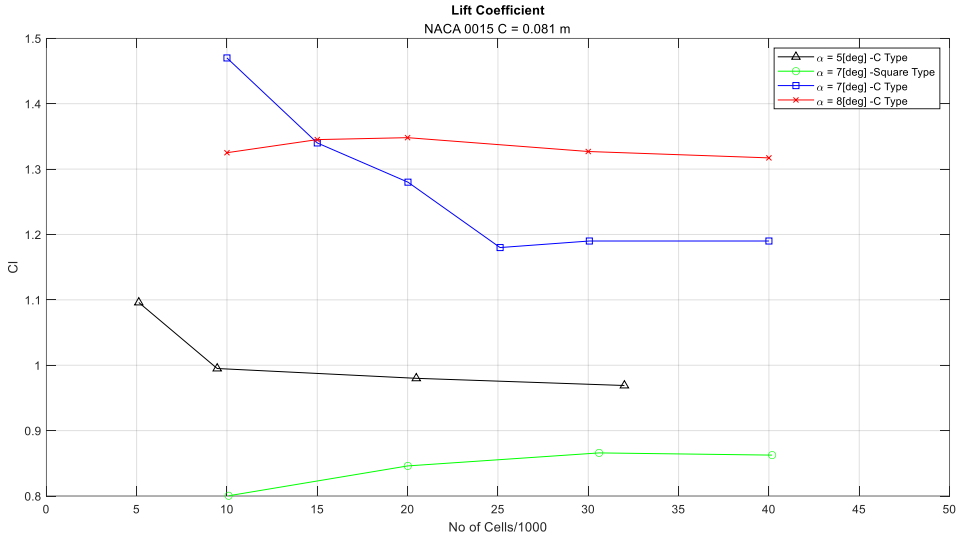

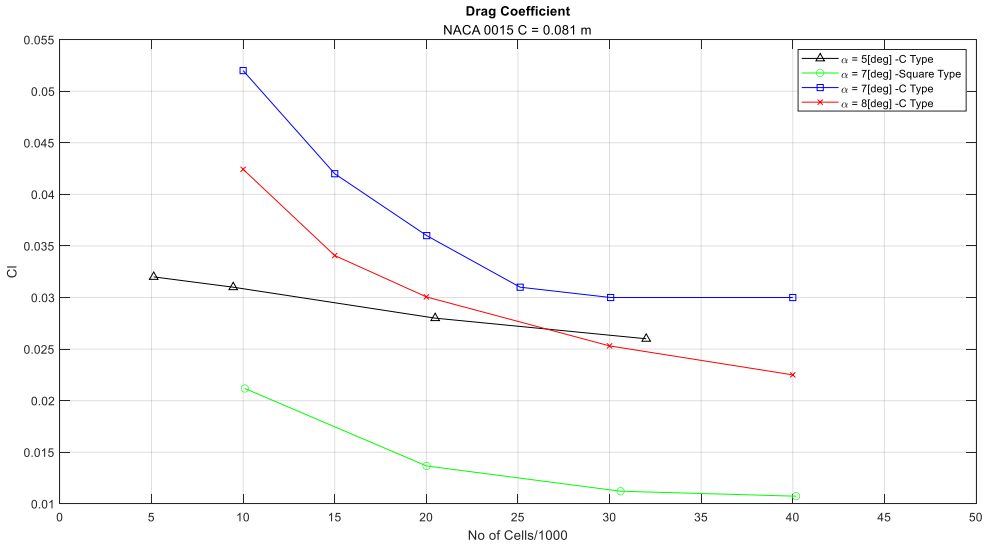

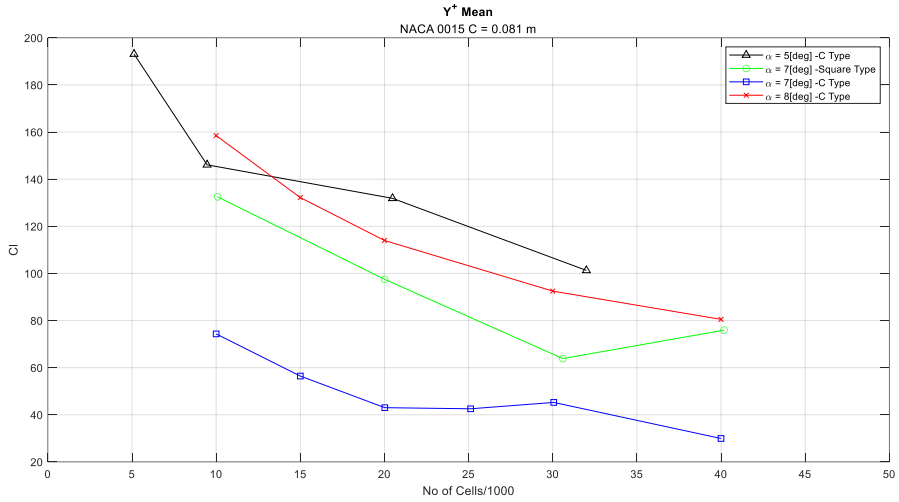

Figure 20.0 Hydrodynamic Coefficients Comparison with Angles of Attack

- **Comparison with the experimental results:**

The results obtained from the different flow conditions and wall treatment are directly compared between the experimental measurements made at SAFL collected at a Reynolds number of approximately 7×10^5 and to Sandia National Laboratories (SNL) at Reynolds numbers of 7×10^5 and 10^6. The difference in the lift and drag coefficient are expressed in terms of percentage.

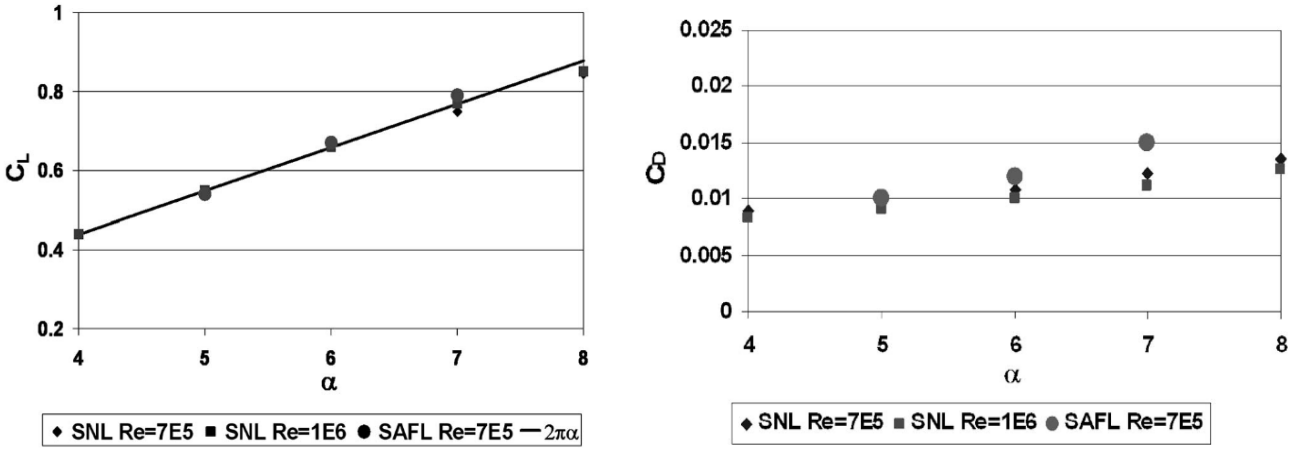

Figure 21.0 Lift and Drag Experimental Results

No of Cells	Domain Size	Conditions	Cl	ΔCl [%] SAFL- 0.8	ΔCl [%] SNL – 0.71	Cd	ΔCd [%] SAFL - 0.015	ΔCl [%] SNL – 0.012
40000	4c/8c	Standard Wall Treatment - SIMPLE FOAM	1.27	58.75	78.87	0.039	160	225
40000	4c/8c	Standard Wall Treatment – PIMPLE FOAM	1.22	52.5	71.83	0.029	93.33	141.67
40000	4c/8c	Scalable Wall Treatment- PIMPLE FOAM	1.19	48.75	67.6	0.030	100	150
37042	4c/8c	Resolved Boundary Layer PIMPLE FOAM	0.7	-12.5	-1.4	0.024	60	100
40000	8c/16c	Standard Wall Treatment - PIMPLE FOAM	1.25	56.25	76.06	0.023	53.33	91.67

Table 8.0: Hydrodynamic Coefficients comparison with experimental results

- **Comparison with domain size and geometry:**

  To obtain extremely precise results, domain boundaries must be placed in such a way that the inner flow field is not disrupted. Due to the fact that there are more meshes in a larger domain, it takes longer to calculate. Therefore, it's crucial to choose a domain size that neither creates an extremely vast domain nor minimizes the effects of the boundaries. The drag estimation is significantly more sensitive to the domain size than the lift estimation. The accuracy of the drag coefficient improves more noticeably than the lift coefficient with an increase in domain size although the number of cells and computation time could significantly rise with additional domain size expansion.

  Also, comparing the results based on the domain geometry, the block- structured H-mesh performs slightly worse than the C-mesh since the C-mesh has better orthogonality around the profile. The lift and drag coefficients were underestimated using the H- mesh and due to the fact that there is increasing difficulty in meshing it falls short of capturing the leading-edge curvature accurately and also propagates the boundary layer in the transverse direction.

  Alongside the wasted use of point clusters and high aspect ratio cells, the high clustered cells both parallel and perpendicular in regions where the flow accelerates can result in significant time step reductions due to CFL conditions, leading to slowing of solver convergence.

  The table below shows the variation of the lift and drag coefficient to the domain sizes in comparison to the experimental results.

No of Cells	Domain Size	Conditions	Cl	ΔCl [%] SAFL- 0.8	ΔCl [%] SNL – 0.71	Cd	ΔCd [%] SAFL - 0.015	ΔCl [%] SNL – 0.012
40000	4c/8c	Standard Wall Treatment – PIMPLE FOAM	1.22	52.5	71.83	0.029	93.33	141.67
40000	8c/16c	Standard Wall Treatment - PIMPLE FOAM	1.25	56.25	76.06	0.023	53.33	91.67
40000	50c/100c	Standard Wall Treatment - PIMPLE FOAM	1.03	28.75	45.07	0.016	6.67	33.33

Table 9.0: Hydrodynamic Coefficients comparison with domain size

- **Comparison with wall treatment type:**

Lift Coefficients:

The Lift Coefficients for the k-ω SST turbulence models for both domain sizes are in good agreement with experimental data at the considered AoA 7 degree. In particular, resolving the boundary layer has shown good estimates amongst the standard and scalable wall functions.
The challenge with resolving the boundary layer is the fact that it is highly computationally expensive.

Drag Coefficients:
For the prediction of the drag coefficient, there is slight discrepancies between the domain sizes. Since the drag coefficient is mesh dependent, the larger the domain size, the closer the Cd is to the experimental data.
The Cd is also more accurately predicted when resolving the boundary layer, and when compared to the standard or scalable wall functions.

Pressure Coefficients:
The coefficient of pressure difference is much larger on the front edge than the rear edge, thus indicates that the lift force of the hydrofoil is mainly generated from the front edge which is likely to be the same when compared to the experimental data, this shows the ability of k-ω SST model to predict accurate pressure distribution around the hydrofoil surface.

In conclusion:

- In terms of computational cost:
  - Since there is little variation in the hydrodynamic coefficient in computing both steady and unsteady conditions using the wall function. For faster approximation the steady state (SIMPLE FOAM) is highly recommended as it favors less computation time and cost.
  - A domain size of 8c around and 16 c after the profile achieves a good balance in both accuracy and efficiency. This domain size is large enough to obtain sufficiently accurate estimates of lift and drag.

- Increasing turbulence intensity and the viscosity ratio yielded no significant change in the CL and Cd, neither did it show any vortex shedding. This is mainly due to the low angle of attack.

7.0. REFERENCES

1. Aerodynamic Characteristics of the NACA 0012 Airfoil Section. Tech. rep., Langley Research Center, Hampton, Virginia, USA.
2. Aftosmis, M. G. D., Tavares, T. S. (1995). Behavior of linear reconstruction techniques on unstructured meshes. AIAA Journal, 33(11), 1–51.
3. Eleni, D. C., Athanasios, T. I., Dionissios, M. P., (2012). Evaluation of the turbulence models for the simulation of the flow over a National Advisory Committee for Aeronautics (NACA) 0012 airfoil. Journal of Mechanical Engineering Research 4 (3), 100–111.
4. Ladson, C. L. (1988). Effects of Independent Variation of Mach and Reynolds Numbers on the Low-Speed
5. Liseikin, V. D. (2009). Grid Generation Methods, 2nd Edition. Springer.
6. Lutton, M. J., (1989). Comparison of C-and O-grid Generation Methods Using a NACA 0012 Airfoil. Master thesis, Air Force Institute of Technology.
7. Kim, H. J., Sang H., K., Jung K. O., and Dae, W. S. (2012). A proposal on standard rudder device design procedure by investigation of rudder design process at major Korean shipyards. Journal of Marine Science and Technology 20 (4): 450–458.
8. Menter, F. Two-equation eddy-viscosity turbulence models for engineering applications. 583 AIAA Journal. 32 1598 1605 (1994).
9. Narsipur, S., Pomeroy, B. W., Selig, M. S., 2012. CFD analysis of multi-element airfoils for wind turbines. In: 30th AIAA Applied Aerodynamics Conference. New Orleans, Louisiana, pp. 1–18.
10. Roberts, T. W., (1990). Prospects for drag prediction using computational fluid dynamics. In: Aerospace Technology Conference and Exposition. Long Beach, CA, USA.
11. Ship Rudder Performance Compared to Wind Tunnel Measurements. Tech. rep., University of Southampton, Southampton, UK.
12. Stuck, A., Turnock, S., Bressloff, N., (2004). An Evaluation of the RANS Method for the Prediction of Steady.
13. Tveiterås, V., (2011). Numerical study of the interaction of flow over two airfoils in relative motion. Master thesis, Norwegian University of Science and Technology.
14. Van Nguyen, T., Ikeda, Y., (2014). Development of fishtail rudder sections with higher maximum lift coefficients. In: 24th International Ocean and Polar Engineering Conference. Busan, Korea, pp. 940–947.
15. Van Nguyen, T., Ikeda, Y., (2013). Hydrodynamic characteristic of rudder sections with high lift force. Journal of the Japan Society of Naval Architects and Ocean Engineers (19), 403–406.
16. Wasberg, C. E., Reif, B. A. P., (2010). Hydrodynamical Simulations in Fluent. Tech. rep., Norwegian Defence Research Establishment (FFI), Kjeller, Norway.